Thermodynamic analysis of nucleation of carbon deposits on metal particles and its implications for the growth of carbon nanotubes

Vladimir L. Kuznetsov,* Anna N. Usoltseva, and Andrew L. Chuvilin
Boreskov Institute of Catalysis, Lavrentieva 5, 630090 Novosibirsk, Russia

Elena D. Obraztsova
Natural Science Centre of Russian Academy of Sciences, 38 Vavilov Street, 117942 Moscow, Russia

Jean-Marc Bonard
Institut de Physique Expérimentale, Ecole Polytechnique Fédérale de Lausanne, CH-1015 Lausanne EPFL, Switzerland
(Received 13 June 2000; revised manuscript received 27 March 2001; published 2 November 2001)

By considering the catalytic mechanisms underlying the formation of various nanocarbon deposits on catalytic metal surfaces, we conclude that the majority of these mechanisms include some common steps. The most important of these is the nucleation of the carbon deposit on the metal surface. On the basis of experimental and literature data, we propose that the nucleus has the form of a flat saucer with its edges bonded to the metal surface. A thermodynamic analysis of the carbon nucleation on the metal surface is then performed to obtain an analytical equation for the dependence of the critical radius of the nucleus on the reaction parameters. This equation demonstrates that a variation of the reaction parameters, such as the temperature and the nature of the metal catalyst and promoters, can lead to the formation of different carbon deposits, such as filamentous carbon, multiwall nanotubes or single-wall nanotubes (SWNTs). The performed analysis allows us to conclude that SWNT growth is likely to proceed on liquid metal particles.

DOI: 10.1103/PhysRevB.64.235401 PACS number(s): 61.48.+c, 68.37.−d, 82.60.Nh

I. INTRODUCTION

The formation of carbon filaments by the catalytic decomposition of carbon-containing gases on a metal surface has been known for a long time. Chemical vapor deposition (CVD) has been used for at least four decades for the production of filamentous carbon by the decomposition of carbon monoxide (CO) or hydrocarbons on metal catalysts.[1–3]. During the past ten years methods for the production of a new type of carbon structures, namely carbon nanotubes, have been developed. These techniques are based on the coevaporation of pure graphite and metal catalysts either in an electric arc discharge[4,5] or by laser ablation.[5,6] Subsequently, the catalytic decomposition of CO and hydrocarbons over supported catalysts was also successfully used for nanotube synthesis. Using the aforementioned techniques, four classes of fibrous carbon deposit have been produced, namely, carbon fibers, filaments, multiwall nanotubes (MWNTs) and single-wall nanotubes (SWNTs). The nanotubes have attracted great attention because of their unusual properties and numerous potential applications.[7] However, the available techniques allow only poor control over the growth of the nanotubes, and yield numerous byproducts such as amorphous carbon, polyhedral carbon nanoparticles, and carbon-encapsulated catalyst particles. The separation of nanotubes from impurities is a difficult task, mainly because the reactivity of the nanotubes is similar to that of the byproducts, and nanotubes may thus be damaged or destroyed during purification procedures. An understanding of the formation mechanism of nanotubes is therefore crucial when designing techniques for the controlled production of pure nanotube material.

In order to understand better the phenomena involved in the formation of different carbon deposits, here we present a thermodynamic analysis of the carbon nucleation at a metal surface. This analysis is based on a consideration of the mechanisms involved in the catalytic formation of the different forms of carbon, and on the conclusion that carbon nucleation at a metal surface is a common step of these mechanisms. A flat saucerlike form for the initial carbon nucleus is proposed after an analysis of our results and published experimental results. The thermodynamic analysis performed allows us to estimate the influence of reaction parameters on the nucleation step, which is a crucial stage for the formation of different carbon deposits.

II. MECHANISMS OF FORMATION OF CARBON DEPOSITS ON METAL PARTICLES

Various mechanisms have been proposed for the formation of filamentous carbon deposits. These mechanisms can be divided into several groups.

(1) In the first group, one can cite mechanisms which include a stage of carbon dissolution that is independent of the carbon source (hydrocarbon or CO decomposition, or graphite vaporization). Baker *et al.*, in 1972, suggested such a mechanism for the formation of filamentous carbon deposits on isolated metallic particles by the catalytic decomposition of hydrocarbons.[8] They proposed that temperature and concentration gradients are the main driving forces for this process. According to this mechanism, hydrocarbons decompose on the exposed surfaces of metal particles, leading to the release of hydrogen as a gas and to the dissolution of carbon in the particle. A temperature gradient results from overheating of part of the catalyst particle during the exothermal hydrocarbon decomposition reaction, and gives rise

to a gradient in the carbon concentration in the volume of the catalyst particle. The dissolved carbon diffuses through the particle and precipitates on the cooler surface of the metal particle. The diffusion of carbon through the catalyst particle is believed to be the rate-limiting step in the growth of filaments.

Note that under the conditions encountered in the arc discharge and laser vaporization, a temperature gradient occurs due to the diffusion of the particles away from the hot zone of the interelectrode plasma or of the vaporization plume. In this case, the carbon precipitation is caused by the decrease in temperature, and hence in carbon solubility.

(2) The second group consists of mechanisms based on the diffusion of carbon at the surface of the metal particle rather than on the bulk diffusion of carbon through the catalyst particle.[9] Such a mechanism leads to the formation of deposits with diameters close to those of the metallic particles. However, the surface diffusion of carbon structures without dissolution of carbon in the metal particle seems improbable. For example, Krivoruchko *et al.*[10] observed by *in situ* TEM that the interaction between iron particles and amorphous carbon at 920 K results in the dissolution of carbon and the migration of liquidlike metal particles with formation of graphitic carbon shells.

(3) Some authors suggested that catalyst particles take part only in the tube initiation process.[7] According to this model, a metal particle initiates the formation of a primary tube, which consists of prefect graphitic layers rolled cylindrically around the metal particle. The thickening of the primary tube by carbon deposition on the outer surface of the tube proceeds without any further participation of the metal particle. Note that this mechanism can be realized only in the presence of free carbon atoms in the gasphase.

(4) For SWNTs, a growth mechanism was proposed where small metal clusters activate SWNT growth by moving around the open tube tip and bonding carbon atoms from the gas phase.[11] This mechanism does not explain the formation of nanotube ropes, which are predominantly observed in SWNT deposits. Although it is possible that this growth mode also takes place during the synthesis, its contribution to the SWNT formation is probably negligible.

(5) A model for the formation of cylindrical layers around a hollow core using a thermodynamic approach was suggested by Tibbetts.[12] In this model, graphitic planes are elastically strained to form a tree-ring structure. This gives rise to an extra elastic term in the considered free-energy equation. However, according to this model the free-energy change prevents the formation of carbon filaments with an inner radius smaller then 5 nm, and the synthesis of carbon nanotubes of much smaller diameter cannot be explained.

In our opinion, such a thermodynamic approach is very promising for the description of the growth of filamentous carbon deposits, but the model suggested by Tibbetts must be extended to include the formation of the carbon nucleus. We suggest that carbon nucleation is a common and crucial step for the formation of all types of filamentous carbon deposits. It determines the critical size of the carbon nucleus and thus the type of carbon deposit obtained, because the size of the tubes or of the graphite plates (in the case of filamentous carbon) cannot be smaller than the critical size of the carbon nucleus.

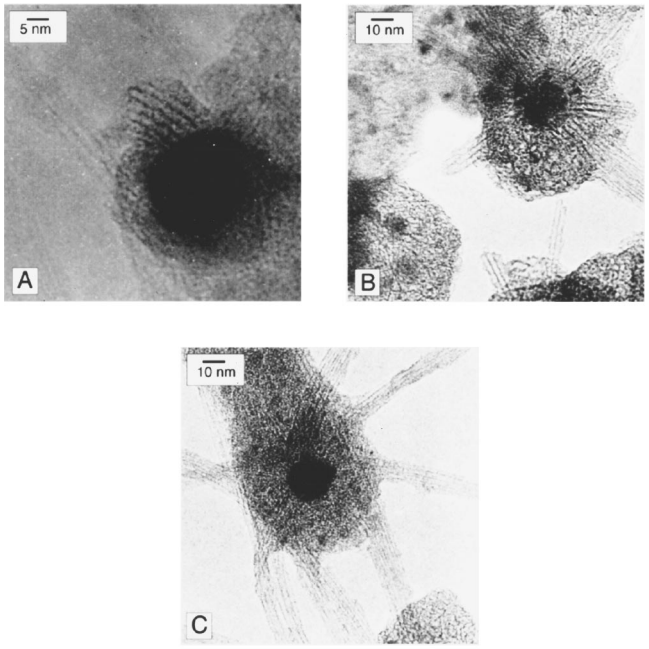

FIG. 1. High-resolution TEM images of ''sea urchin'' particles: (a) initial step of SWNT growth, (b) intermediate step, (c) and final state. The SWNT samples were prepared by arc discharge between two graphite electrodes, one of which was filled with a mixture of Ni, Y_2O_3, and graphite powder (Ref. 17). For structural investigation we used pristine soot samples without any purification treatment. The specimens were prepared by ultrasonic dispersion of the carbon deposit in ethanol, and subsequent application of a drop of the suspension on a holey carbon grid.

When the critical radius of the carbon nucleus is considerably smaller than that of the metal particle and the saturation of the metal-carbon particles by carbon is sufficiently high, the formation of several nuclei is possible. These nuclei can grow independently and can reach a size which allows them to interact with each other. This interaction results in the formation of mosaic structures consisting of growing nuclei. ''Sea-urchin'' particles, which consist of SWNT ropes growing radially from metal or metal carbide particles encapsulated in graphitic shells, in our opinion represent an example of such structures. The presence of such particles was demonstrated earlier,[13–16] and we also observed these particles in typical soot samples obtained by the arc discharge method[17] (Fig. 1). Note that on our TEM images the length of the nanotubes extending from the particle is variable and depends on the considered particle. This strongly suggests that they represent different stages of SWNT growth, such as on Fig. 1(a) for the initial step (nucleation and growth of short tubes), Fig. 1(b) for an intermediate step (radial extension of the tubes), and Fig. 1(c) for the final state (formation of ropes of more than 1 μm length).

III. THERMODYNAMIC ANALYSIS OF FACTORS AFFECTING THE CRITICAL RADIUS OF THE NUCLEUS

We suggest that at the beginning of the nucleation a few carbon atoms precipitate on the surface of carbon-saturated

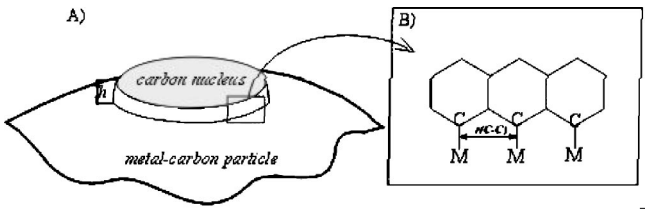

FIG. 2. Schematics of the two-dimensional carbon nucleus on the surface of the catalyst metal particle.

metal particles. They combine into small structures with carbon atoms arranged in hexagons, which transform into a graphene sheet bonded with its edges to the metal surface (Fig. 2). This form of the nucleus is most favorable because of the elimination of dangling bonds in the carbon cluster. The nucleus grows with the addition of precipitating carbon atoms to the edges of the nucleus. Note that a similar structure was proposed by Tontegode and co-workers[18,19] on the base of their theoretical data. Furthermore, such flat carbon nanoobjects, two layers in thickness, 45 Å of average diameter and located on the step edge of metal (Pd) terraces, were observed and characterized recently by scanning tunnelling microscopy.[20] The exposed lower carbon layer of these structures was embedded in the surface plane of Pd, and presents a ring-shaped atomic structure similar to a single graphite layer. After formation of the nucleus, the tube can grow according to several scenarios.

In the first scenario, the nucleus continues to grow, which results in the formation of graphitic sheets covering a significant part of the surface of the metal particle. This growth and the forthcoming exfoliation of the graphitic sheet induces produces a variety of filamentous structures,[21] with graphitic sheets that are oriented at an angle or perpendicular to the fiber axis (called fibers or filaments).

In the second scenario, new nuclei form under the primary one, with edges that are bonded to the surface of the metal particle. The central part of this multilayered nucleus begins to separate from the surface as soon as it reaches a critical size that determines the diameter of the tubular deposit. This scenario leads to the formation of a MWNT. Usually, the external walls have a diameter that is comparable to the size of the metal particle. Note that the internal tube radius cannot be smaller than the critical radius of the nucleus that is characteristic for the experimental conditions (see below).

In the third scenario, several nuclei precipitate on the surface of the same metal particle, and increase in diameter until they interact to form a tightly packed mosaic structure, which can develop to form nanotube ropes. If the nucleation frequency is high enough, the size of a single nanotube tends toward a minimal value that corresponds to the critical radius of the nucleus.

In the following we consider only the nucleation steps, and leave the kinetic aspects of nucleation for further analysis. Let us consider the simplest model of carbon nucleation. The change in Gibbs free energy in the case of the formation of a two-dimensional nucleus (with perimeter l and height h) can be written as[22]

$$\Delta G = \frac{\gamma l^2 h}{V_m}\Delta G_{\text{nucleus}} + \gamma l^2(\sigma_{\text{nucleus-gas}} + \sigma_{\text{nucleus-surface}} - \sigma_{\text{surface-gas}}) + l\epsilon + E_{\text{str}}, \quad (1)$$

where γl^2 is the surface area of the nucleus, γ is a geometrical factor determined by the form of the nucleus, and V_m is the molar volume of graphite. $\Delta G_{\text{nucleus}}$ represents the change in free energy following the precipitation of 1 mol of carbon from the metal-carbon solution:

$$\Delta G_{\text{nucleus}} = -RT\ln(a/a_0) = -RT\ln(x/x_0). \quad (2)$$

a_0 and a are the carbon activities of the saturated and actual solutions, respectively, and a/a_0 is the saturation coefficient of the solution. Correspondingly, x_0 and x are the saturated and actual molar content of the dissolved carbon, respectively, and $x/x_0 = a/a_0$. Finally, ϵ is the specific edge free energy (J/m), σ is the corresponding specific surface energy (J/m^2), and E_{str} is the strain energy that arises from the bending of the graphene layer during bonding with the metal surface. It can be described using the continuum elasticity formalism[23,24] (see Appendix A), and is in our case equal to $E_{\text{str}} = Q_c l/4.5h$, with $Q_c = 4.4$ eV.[23] Equation (1) can thus be rewritten as

$$\Delta G = \frac{\gamma l^2 h}{V_m}\Delta G_{\text{nucleus}} + \gamma l^2(\sigma_{\text{nucleus-gas}} + \sigma_{\text{nucleus-surface}} - \sigma_{\text{surface-gas}}) + l\epsilon + \frac{Q_c l}{4.5h}. \quad (3)$$

The maximum of ΔG as a function of l corresponds to the critical size of the nucleus, and is expressed from Eq. (3) as

$$\frac{d\Delta G}{dl} = 2l\left[\frac{\gamma h}{V_m}\Delta G_{\text{nucleus}} + \gamma(\sigma_{\text{nucleus-gas}} + \sigma_{\text{nucleus-surface}} - \sigma_{\text{surface-gas}})\right] + \epsilon + \frac{Q_c}{4.5h} = 0,$$

from which we easily deduce

$$l_{\text{crit}} = -(\epsilon + Q_c/4.5h)(2[(\gamma h/V_m)\Delta G_{\text{nucleus}} + \gamma(\sigma_{\text{nucleus-gas}} + \sigma_{\text{nucleus-surface}} - \sigma_{\text{surface-gas}})])^{-1}.$$

If we further consider only circular nuclei with $l = 2\pi r$ and $\gamma = 1/4\pi$, we obtain

$$r_{\text{crit}} = -(\epsilon + Q_c/4.5h)[-(h/V_m)RT\ln(x/x_0) + (\sigma_{\text{nucleus-gas}} + \sigma_{\text{nucleus-surface}} - \sigma_{\text{surface-gas}})]^{-1}. \quad (4)$$

In order to estimate the critical radius in the temperature range of 773–1470 K, which is typical for the formation of catalytic carbon deposits, we use the following approximations. $\sigma_{\text{nucleus-gas}}$ and $\sigma_{\text{surface-gas}}$ can be taken as the specific surface energy of the basal plane of graphite, σ_{graph}, and of the metal surface, σ_{metal}, respectively. Note that we do not specify the crystallographic index of the metal surface for σ_{metal}, but instead use the experimental values for the most

stable surfaces under the corresponding experimental conditions. $\sigma_{\text{nucleus-surface}}$ can be estimated as the specific surface energy of metal-graphite interaction, which depends on the work of adhesion of the graphite-metal system and is written as $W_{\text{ad}}=\sigma_{\text{graph}}+\sigma_{\text{metal}}-\sigma_{\text{graph-metal}}$; hence $\sigma_{\text{graph-metal}}=\sigma_{\text{graph}}+\sigma_{\text{metal}}-W_{\text{ad}}$. With these approximations Eq. (4) becomes

$$r_{\text{crit}}=\frac{-(\epsilon+Q_c/4.5h)}{-(h/V_m)RT\ln(x/x_0)+(2\sigma_{\text{graph}}-W_{\text{ad}})}. \qquad (5)$$

Equation (5) expresses the dependence of the critical radius on the different reaction parameters. The radius decreases with increasing temperature (T), with increasing saturation coefficient of the metal-carbon solution (x/x_0), and with decreasing specific edge free energy (ϵ). Note that this criterion gives us a minimal value for the radius of the carbon nucleus. Nuclei with smaller radii are not stable, but nuclei with larger sizes can continue to grow.

In our model, the carbon atoms at the edge of the nucleus differ from the central atoms. Each of the former is bonded with one metal atom and two carbon atoms, in contrast to the latter that are bonded with three carbon atoms. The specific edge free energy ϵ therefore determines the energy difference required for the chemical bonding of the border atoms with the metal surface. The value of ϵ can be estimated as the difference between the enthalpies of formation of carbon-carbon and metal-carbon bonds, divided by the distance between two neighboring carbon atoms, $r_{\text{C-C}}$, in the zigzag edge of a graphite sheet as shown on Fig. 4(b) (for more detailed considerations, see Appendix B):

$$\epsilon=\frac{\Delta H_{M\text{-C}}-\Delta H_{\text{C-C}}}{2N_A r_{\text{C-C}}}.$$

Let us estimate numerically the critical radius given by Eq. (5) for pure iron and nickel catalysts. The enthalpy of the carbon-carbon bond in graphite is equal to -473.2 kJ/mol,[25] and the enthalpy of the metal-carbon bond for Fe and Ni is equal to -245.2 and -191.2 kJ/mol, respectively.[26] The values of the specific edge free energy are equal to 1.51×10^{-19} and 1.88×10^{-19} J/Å for iron and nickel, respectively. Note that the estimates of ϵ depend on the values of the metal-carbon bond enthalpies used. There is a large spread for the values reported in the literature by different authors depending on the calculation or experimental methods.[27–29]

The height of the nucleus, h, can be estimated by the interlayer distance in graphite (3.4 Å), and $r_{\text{C-C}}$ is equal to 2.5 Å. The molar volume of graphite is 5.3×10^{-24} Å^3/mol. The specific surface energy for the basal plane of graphite, σ_{graph}, is 0.077 J/m^2 at 1243 K.[30] The work of adhesion of graphite on the solid metal surface, W_{ad}, is in the range 0.04–0.14 J/m^2.[31]

In fact, the value of W_{ad} and of the degree of carbon saturation, x/x_0, considerably change when the temperature increases from 700 to 1700 K because both parameters strongly depend on the state of the metal-carbon mixture (liquid or solid solution). Conversely, the values of ϵ and σ_{graph} are not significantly affected by an increase of the temperature. The melting point of pure iron and nickel (1812 and 1728 K, respectively), and their carbides lie beyond the temperature region typical for carbon fibers and nanotubes formation (700–1500 K). However, the melting point of the Fe-C and Ni-C eutectics lie in this region, and are equal to 1403 and 1584 K, respectively.

The existence of an ''oversaturated'' metal-carbon solution results from contacts of metal with carbon atoms that are less stable than graphite (for example, the atoms of carbon vaporized in the arc discharge, or amorphous and ''active'' carbon just after formation on the catalyst metal surface after hydrocarbon or CO decomposition reaction). The upper limit of supersaturation x/x_0 was estimated in Ref. 32 from the difference of chemical potentials between amorphous carbon and graphite as equal to 4. However, other estimations and experimental data on metal-carbon eutectics shifts[33] gave a significantly smaller value ($x/x_0\approx1.5-2$). We therefore used $x/x_0=2$ in our estimation.

Since near 1400–1500 K—and probably also at lower temperature[28]—metal particles can exist in a liquid state, the carbon content in the solution can be increased and W_{ad} is also changed. The values of W_{ad} for transition-metal melts are considerably higher than for the solid state. For iron and nickel melts saturated with carbon (graphite), the work of adhesion is equal to 2.2 and 1.8 J/m^2, respectively.[34] These values correspond to metal-carbon eutectics, with carbon contents of about 17 at. % (for Fe) and 10 at. % (for Ni). Note that for pure metals the values of W_{ad} are 3.6 and 3.0 J/m^2 (for Fe and Ni, respectively) and they decrease when the carbon content increases.[34]

Our numerical results for the critical radius of carbon nucleus as a function of reaction temperature are presented in Fig. 3. Note that for the estimates of r_{crit} for solid metal particles we have used a medium value of $W_{\text{ad}}=0.1$ J/m^2. The variation of this value within the range typical for solid metals (0.04–0.14 J/m^2)[31] does not change significantly the value of r_{crit} (±3 Å at a fixed temperature). The critical radius for a liquid metal particle is much smaller than for a solid particle due to a much higher W_{ad} for metal melts. The change of the state of the particles occurs at temperatures close to the corresponding metal-carbon eutectic temperatures.

The estimates obtained in Fig. 3 are in good agreement with the experimental data presented in Table I and reproduced in Fig. 3. The table summarizes the results reported in the literature on the relationship between the average diameter of tubular carbon deposits, the nature of the metal catalysts, and the reaction temperature. Based on these data one can identify three separate temperature regions that correspond to three different types of carbon products. From 773 to 993 K, fibers with diameters 250–1500 Å are obtained. Multiwall nanotubes with inner diameters of 30–100 Å are formed at 773-1373 K, and above 1373–1473 K single-walled nanotubes with diameters 7–20 Å are synthesized. This tendency coincides nicely with the variation of the critical radius with the reaction temperature estimated from Eq. (5). For more clarity, we marked the values extracted from the literature[6,13,35,37,38,41–43,45–50] in Fig. 3 for Fe and Ni cata-

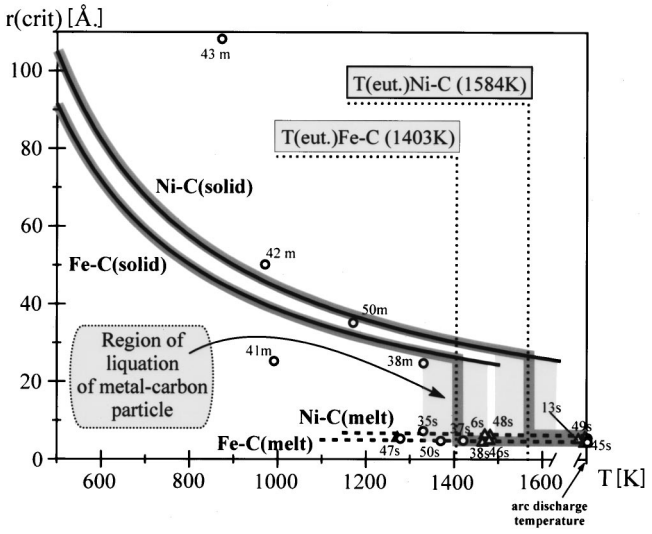

FIG. 3. Dependence of the critical radius of the carbon nucleus on the reaction temperature according to Eq. (4) for Ni and Fe catalysts, along with values extracted from the literature for Fe and Ni catalysts (marked by circles and triangles, respectively). The number refers to the cited paper, and the letter to the type of deposit (*m* for multiwall and *s* for a single wall, respectively). Note that for multiwalled nanotubes and fibers the critical radius corresponds to the minimum possible value of the obtained radius.

lysts by circle and triangle symbols, respectively.

Note that for multiwalled nanotubes and fibers, the critical radius of the carbon nucleus corresponds to the minimum possible radius of the innermost wall, and therefore does not determine the outer radius of the obtained deposit. Furthermore, the predicted decrease of tube diameter with increasing temperature is valid only for the nucleation step. At later stages of the growth, the diameter may increase with the temperature, as predicted by other models[6] and verified experimentally.[35,48]

It is worth mentioning that the different temperature regions corresponding to the various deposits do not have precise boundaries, and that different types of products are formed depending on the reaction conditions.[39,41] A comparison of the critical radius calculated for liquid and solid metal particles with the experimental data shows that the liquid state is the most probable in the high-temperature region where SWNT formation is observed. The available data on the influence of an additional promoter on the nanotube yield is another argument in favor of the liquid state of metal-carbon particles.[11] The presence of promoters such as S, Bi, or Pb increases the production yield of SWNTs (and also modifies the diameter distribution) due to a decrease of the melting point of the multicomponent system (catalyst-promoter-carbon) as compared to the catalyst-carbon mixture.

The nature of the metal catalyst can also affect the value of r_{crit}. The use of a metal characterized by a higher metal-carbon bond energy can lead to the formation of tubes with smaller diameter. Different metals will show variations in the carbon solubility as well as in the melting temperature of the metal-carbon mixtures. Obviously, further experimental data are needed to better understand the influence of the metal

TABLE I. Summary of the results reported in the literature on the relationship between the type and average diameter of tubular carbon deposits, the nature of the metal catalysts, and the reaction temperature.

Method of synthesis	Catalyst	T (K)	Type of carbon deposit	Diameter (Å)	Ref.
arc discharge	Ni, NiO	>2273	SWNT	10–16	13
arc discharge	La_2O_3	>2273	SWNT	18–21	16
arc discharge	Ni/Y	>2273	SWNT	12–17	35
arc discharge	YC_2	>2273	SWNT	11–17	36
laser ablation	Ph/Pd	>2273	SWNT	6.8–14.3	14
CVD	Fe	1373–1473	SWNT	16.9	37
laser ablation	Ni/Co	1473	SWNT	13.8–20.0	6
CVD	Mo/Al_2O_3, $Ni+Co/Al_2O_3$	1473	SWNT	10–50	38
CVD	Fe/Al_2O_3	1323	MWNT	50–150	39
			SWNT	≈ 15	
CVD+ laser ablation	Ni	1023	MWNT	$d_{\mathrm{in}}=30$-100	40
CVD	(Co, Fe, Cu)/ SiO_2	973	MWNT	$d_{\mathrm{in}}=40$–70	41
CVD	or zeolites		SWNT	10	
CVD	Fe	923–1073	MWNT	$d_{\mathrm{in}}=50$–80	42
CVD	(Fe, Co, Ni, Cu)/ C or SiO_2	773–1073	MWNT	$d_{\mathrm{in}}=30$–100	43
CVD	Fe, Fe/Cu, Fe/SiO_2	873	fibers	900–1600	21
CVD	Co/Ni	873	fibers	240–280	44

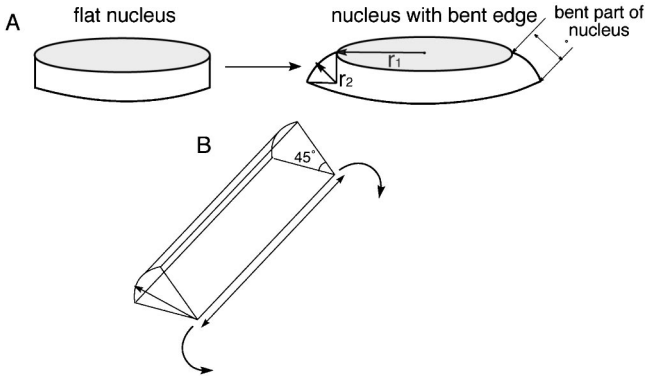

FIG. 4. Schematics of the deformation of the carbon nucleus bonded to the metal surface.

nature and impurities on the nucleation of carbon nanotubes, and we believe that our simple model may provide important clues for future studies.

IV. CONCLUSION

We suggest that the stage of carbon nucleation on the surface of the metal catalyst is common for all types of carbon deposits. The difference in morphology of the carbon deposits depends on the reaction conditions and on the nature of the metal catalyst. A thermodynamic analysis of the influence of different reaction parameters on the critical radius of the carbon nucleus was performed, allowing us to draw the following conclusions.

(1) An increase of the temperature leads to the formation of smaller nuclei, and finally to the formation of SWNTs.

(2) The use of metals characterized by a higher metal-carbon energy bond yields nanotubes with smaller diameters.

(3) SWNT growth is likely to proceed on liquid metal particles.

(4) Elements that decrease the melting point of the catalyst-carbon mixture and do not form stable compounds with carbon at the reaction temperature also promote the formation of SWNTs.

ACKNOWLEDGMENTS

The authors thank Dr. V. N. Parmon and Dr. N. M. Bazhin for fruitful discussion. This work was supported by INTAS Grant No 97-1700.

APPENDIX A: ESTIMATION OF DEFORMATION ENERGY

To estimate the deformation energy, we consider a nucleus with a flat central part and a curved edge bonded to the metal surface as a representative plausible geometry. The edge is bent in each point in two perpendicular directions. We can thus take into consideration the strain energy caused by the bending of the nucleus surface with two radii of curvature. [Fig. 4(a)]. The first (r_1) is equal to the radius of the nucleus. The second (r_2) is constant and equal to h, the distance between the graphene nucleus and the metal surface. The contribution to the strain energy of the first type of bending is significantly less than that of the second type.

Hence we consider that the strain energy arises only from the second type of bending. The curved edge surface can be described as the part of cylinder with radius $R=h$ and height $H=l$ [where l is the perimeter of the nucleus, Fig. 4(b)].

We propose that the strain is distributed within an arc consisting of a six fold graphene ring band. The length of this arc is approximately equal to 4.8 Å. The bent part of the nucleus is approximately equal to 1/4.5 of the cylinder. According to the continuum elasticity formalism[23] for uncapped cylinders of radius R and length H, the total strain energy compared with a flat graphene sheet is approximately $E_{\mathrm{str}}=Q_c H/R$,[23,24] where Q_c is constant and equal to 4.4 eV in the case of an uncapped cylinder.[23] Since in our model the bending part of the nucleus can be estimated as 1/4.5 of the cylinder, the strain energy of the nucleus can be written as $E_{\mathrm{str}}=Q_c l/4.5h$.

APPENDIX B: ESTIMATION OF SPECIFIC EDGE FREE ENERGY

The change in Gibbs free energy for the nucleus can be written as a combination of two parts: $\Delta G_{\mathrm{nucleus}}=\Delta G_{\mathrm{flat}}+\Delta G_{\mathrm{edges}}$, where ΔG_{flat} and $\Delta G_{\mathrm{edges}}$ is the free-energy change of the flat part of the nucleus and of the nucleus edges bonded with the metal surface, respectively. If N is the total number of carbon atoms of the nucleus, and n the number of edge atoms bonded with one metal and two carbon atoms, $(N-n)$ is the number of central atoms bonded with three carbon atoms. Taking into consideration that $\Delta G=\Delta H-T\Delta S$,

$$\Delta G_{\mathrm{nucleus}}=\frac{3}{2}(N-n)\Delta H_{\mathrm{C\text{-}C}}-\frac{3}{2}(N-n)T\Delta S_{\mathrm{C\text{-}C}}+n\Delta H_{\mathrm{C\text{-}C}}$$

$$+\frac{n}{2}\Delta H_{M\text{-}\mathrm{C}}-nT\Delta S_{\mathrm{C\text{-}C}}-\frac{n}{2}T\Delta S_{M\text{-}\mathrm{C}}$$

where $\Delta H_{\mathrm{C\text{-}C}}$ and $\Delta H_{M\text{-}\mathrm{C}}$ are the enthalpies of formation of a single graphite C-C and metal-carbon bonds, respectively, and $\Delta S_{\mathrm{C\text{-}C}}$ and $\Delta S_{M\text{-}\mathrm{C}}$ are the corresponding values of the entropy of formation. $\Delta S_{\mathrm{C\text{-}C}}$ and $\Delta S_{M\text{-}\mathrm{C}}$ are comparable and taken as equal to the value for sp^2 carbon atoms due to the similarities in the carbon coordination in both cases. We obtain

$$\Delta G_{\mathrm{nucleus}}=\frac{3}{2}N\Delta H_{\mathrm{C\text{-}C}}-\frac{3}{2}NT\Delta S_{\mathrm{C\text{-}C}}-\frac{n}{2}\Delta H_{\mathrm{C\text{-}C}}+\frac{n}{2}\Delta H_{M\text{-}\mathrm{C}}$$

$$=N\Delta G_N+\frac{n}{2}(\Delta H_{M\text{-}\mathrm{C}}-\Delta H_{\mathrm{C\text{-}C}})$$

Taking into consideration that $N=\gamma l^2 h/V_m$ and that $(n/2)(\Delta H_{M\text{-}\mathrm{C}}-\Delta H_{\mathrm{C\text{-}C}})$ can be expressed as $l(\Delta H_{M\text{-}\mathrm{C}}-\Delta H_{\mathrm{C\text{-}C}})/(2r_{\mathrm{C\text{-}C}})=l\epsilon$, the change in Gibbs free energy can be written as

$$\Delta G_{\mathrm{nucleus}}=\frac{\gamma l^2 h}{V_m}\Delta G+l\epsilon.$$

*Electronic address: kuznet@catalysis.nsk.su

[1] L.V. Radushkevich and V.M. Lukyanovich, Zh. Fiz. Khim. **26**, 88 (1952).
[2] L.J.E. Hofer, E. Sterling, and J.T. McCartney, J. Phys. Chem. **59**, 6210 (1955).
[3] M.S. Dresselhaus, G. Dresselhaus, K. Sugihara, I.L. Spain, and H.A. Goldberg, *Graphite Fibers and Filaments* (Springer-Verlag, Berlin, 1988).
[4] S. Iijima, Nature (London) **354**, 56 (1991).
[5] C. Journet and P. Bernier, Appl. Phys. A: Mater. Sci. Process. **67**, 1 (1998).
[6] A. Thess, R. Lee, P. Nikolaev, H. Dai, P. Petit, J. Robert, C. Xu, Y.H. Lee, S.G. Kim, A.G. Rinzler, D.T. Colbert, G.E. Scuseria, D. Tomanek, J.E. Fischer, and R.E. Smalley, Science **273**, 483 (1996).
[7] T.W. Ebbesen, *Carbon Nanotubes: Preparation and Properties* (CRC Press, Boca Raton, FL, 1997).
[8] R.T.K. Baker, M.A. Barber, P.S. Harris, F.S. Feates, and R.J. Waite, J. Catal. **26**, 51 (1972).
[9] A. Oberlin, M. Endo, and T. Koyama, Carbon **14**, 133 (1976).
[10] O.P. Krivoruchko, V.I. Zaikovsky, and K.I. Zamaraev, Dokl. Acad. Nauk **329**, 744 (1993).
[11] C.-H. Kiang and W.A. Goddard III, Phys. Rev. Lett. **76**, 2515 (1996).
[12] G.G. Tibbetts, J. Cryst. Growth **66**, 632 (1984).
[13] Y. Saito, M. Okuda, N. Fujimoto, T. Yoshikawa, M. Tomita, and T. Hayashi, Jpn. J. Appl. Phys. **33**, L526 (1994).
[14] H. Kataura, A. Kimura, Y. Ohtsuka, S. Suzuki, Y. Maniwa, T. Hanyu, and Y. Achiba, Jpn. J. Appl. Phys. **37**, L616 (1998).
[15] S. Subramoney, R.S. Ruoff, D.C. Lorents, and R. Malhotra, Nature (London) **366**, 637 (1993).
[16] Y. Saito, M. Okuda, M. Tomita, and T. Hayashi, Chem. Phys. Lett. **236**, 419 (1995).
[17] E.D. Obraztsova, J.-M. Bonard, V.L. Kuznetsov, V.I. Zaikovslii, S.M. Pimenov, A.S. Pozarov, S.V. Terekhov, V.I. Konov, A.N. Obraztsov, and A.P. Volkov, Nanostruct. Mater. **12**, 567 (1999).
[18] A.Ya. Tontegode and E.V. Rutkov, Solid State Phys. **29**, 1306 (1987).
[19] A.Ya. Tontegode, Surface **8**, 13 (1988).
[20] F. Dulot, J. Eugene, B. Kierren, D. Malterre, and K.N. Eltsov, Phys. Low-Dimens. Semicond. Struct. **1/2**, 217 (1999).
[21] N.M. Rodriguez, A. Chambers, and R.T.K. Baker, Langmuir **11**, 3862 (1995).
[22] B.I. Deryagin and D.V. Fedoseev, Usp. Khim. **39/7**, 1663 (1970).
[23] D. Tomanek, W. Zhong, and E. Krastev, Phys. Rev. B **48**, 15461 (1993).
[24] D.H. Robertson, D.W. Brenner, and J.W. Mintmire, Phys. Rev. B **45**, 12592 (1992).
[25] S.V. Shulepov, *Physics of Carbon Materials* (Metallurgy, Chelyabinsk, 1990) (in Russian).
[26] P.L. Pauson, *Organometallic Chemistry* (Mir, Moscow, 1970).
[27] J.A. Martinho Simoes and J.L. Beauchamp, Chem. Rev. **90**, 629 (1990).
[28] E. Miyazaki, J. Catal. **65**, 84 (1980).
[29] M.J. Filatov, I.L. Zilberberg, and G.M. Zhidomirov, Int. J. Quantum Chem. **44**, 565 (1992).
[30] J. Abrahamson, Carbon **11**, 337 (1973).
[31] G.A. Somorjai, *Introduction to Surface Chemistry and Catalysis* (Wiley, New York, 1994), p. 602.
[32] V.N. Parmon, Catal. Lett. **42**, 195 (1996).
[33] V.B. Fedorov, M.Kh. Shoshorov, O.V. Gusev, I.Kh. Musyaev, N.N. Shipkov, D.K. Khakimova, and N.G. Procenko, in *Fibrous and Dispersion-Strengthened Composition Materials* (Nauka, Moscow, 1976), p. 29 (in Russian).
[34] *Surface Properties of Melts and Solids and their Applications in Science of Materials*, edited by Yu.V. Naidich (Naukova Dumka, Kiev, 1991), p. 64 (in Russian).
[35] K.A. Williams, M. Tachibana, J.L. Allen, L. Grigorian, S.-C. Cheng, S.L. Fang, G.U. Sumanasekera, A.L. Loper, J.H. Williams, and P.C. Eklund, Chem. Phys. Lett. **310**, 31 (1999).
[36] D. Zhou, S. Seraphin, and S. Wang, Appl. Phys. Lett. **65**, 1593 (1994).
[37] H.M. Cheng, F. Li, X. Sun, S.D.M. Brown, M.A. Pimenta, A. Marucci, G. Dresselhaus, and M.S. Dresselhaus, Chem. Phys. Lett. **289**, 602 (1998).
[38] H. Dai, A.G. Rinzler, P. Nikolaev, A. Thess, D.T. Colbert, and R.E. Smalley, Chem. Phys. Lett. **260**, 471 (1996).
[39] A. Peigney, Ch. Laurent, F. Dobigeon, and A. Rousset, J. Mater. Res. **12**, 613 (1997).
[40] H. Kanzow, A. Schmalz, and A. Ding, Chem. Phys. Lett. **295**, 525 (1998).
[41] A. Fonseca, K. Hernadi, P. Piedogrosso, J.-F. Colomer, K. Mikhopadhyay, R. Doome, S. Lazarescu, L.P. Biro, Ph. Lambin, P.A. Thiry, D. Bernaerts, and J.B. Nagy, Appl. Phys. A: Mater. Sci. Process. **67**, 11 (1998).
[42] K. Hernadi, A. Fonseca, J.B. Nagy, D. Bernaerts, and A.A. Lucas, Carbon **34**, 1249 (1996).
[43] V. Ivanov, J.B. Nagy, Ph. Lambin, A. Lucas, X.B. Zhang, X.F. Zhang, D. Bernaerts, G. Van Tendeloo, S. Amelinckx, and J. Van Landuyt, Chem. Phys. Lett. **223**, 329 (1994).
[44] W.B. Downs and R.T.K. Baker, J. Mater. Res. **10**, 625 (1995).
[45] Y. Saito, T. Koyama, and K. Kawabata, Z. Phys. D: At., Mol. Clusters **40**, 421 (1997).
[46] H. Takahashi, M. Sugano, A. Kasuya, Y. Saito, T. Kayama, and Y. Nishina, J. Mater. Sci. Eng. A . **217**, 48 (1996).
[47] L.-C. Qin and S. Iijima, Chem. Phys. Lett. **269**, 65 (1997).
[48] S. Bandow, S. Asaka, Y. Saito, A.M. Rao, L. Grigorian, E. Richter, and P.C. Eklund, Phys. Rev. Lett. **80**, 3779 (1998).
[49] M. Yudasaka, R. Yamada, N. Sensui, T. Wilkins, T. Ichihashi, and S. Iijima, J. Phys. Chem. B **103**, 6224 (1999).
[50] K. Bladh, L.K.L. Folk, and F. Rohmund, Appl. Phys. A: Mater. Sci. Process. **70**, 317 (2000).